

Topology and magnetism in the Kondo insulator phase diagramMichael Klett ¹, Seulgi Ok,² David Riegler ¹, Peter Wölfle ³, Ronny Thomale ^{1,*} and Titus Neupert ^{2,†}¹*Institute for Theoretical Physics and Astrophysics, University of Würzburg, Am Hubland, D-97074 Würzburg, Germany*²*Department of Physics, University of Zurich, Winterthurerstrasse 190, 8057 Zurich, Switzerland*³*Institute for Theory of Condensed Matter, Karlsruhe Institute of Technology, 76131 Karlsruhe, Germany*

(Received 5 December 2019; revised manuscript received 17 February 2020; accepted 24 March 2020; published 21 April 2020)

Topological Kondo insulators are a rare example of an interaction-enabled topological phase of matter in three-dimensional crystals—making them an intriguing but also hard case for theoretical studies. Here, we aim to advance our theoretical understanding by solving the paradigmatic two-band model for topological Kondo insulators using a fully spin-rotation invariant slave-boson treatment. Within a mean-field approximation, we map out the magnetic phase diagram and characterize both antiferromagnetic and paramagnetic phases by their topological properties. Among others, we identify an antiferromagnetic insulator that shows, for suitable crystal terminations, topologically protected hinge modes. Furthermore, Gaussian fluctuations of the slave-boson fields around their mean-field value are included in order to establish the stability of the mean-field solution through computation of the full dynamical susceptibility.

DOI: [10.1103/PhysRevB.101.161112](https://doi.org/10.1103/PhysRevB.101.161112)

Introduction. Landau's theory of spontaneous symmetry breaking and topological phenomena are often cited as two antipodal concepts by which phases of matter can be organized. However, in strongly correlated topological systems, which are surprisingly rare in three-dimensional systems, they can show an intriguing interplay. One of the paradigmatic examples are topological Kondo insulators (TKIs) [1,2], in which d and f electron bands partially overlap and hybridize. This band overlap sources the band inversion central to topological band theory, while correlations from the strongly localized f electrons induce a robust hybridization gap between these bands and thus bring about an insulating ground state.

Several materials fall in this category, with SmB_6 being the best-studied example. The nature of its ground state is still under debate despite intense experimental investigations, with evidence for a topological [3–8] as well as a nontopological [9] scenario, while some works even report indications for a metallic state [10–12]. Another point of controversy is the magnetic order of SmB_6 , with indications for paramagnetic (PM) [13], A-type antiferromagnetic (AFM) [8,14], Neel-AFM [9,15,16], and surface-ferromagnetic phases. The presence of magnetism would crucially influence the topological classification of the material. Jointly, these results demonstrate that SmB_6 and, more broadly, TKIs are at a nontrivial intersection of topology, symmetry-breaking, and correlated phenomena.

This renders the systems not only as highly relevant but also an intrinsically hard case for theoretical studies. Analytical and numerical methods are challenged by a strongly correlated interplay between localized and delocalized as well as spin and orbital degrees of freedom. In this work, we adopt

Kotliar-Ruckenstein's formulation of the slave-boson formalism [17], which matches with the Gutzwiller approximation in infinite dimensions, to map out its magnetic and topological phase diagram. We use Kotliar and Ruckenstein's scheme among the many variants of slave-boson formulations because it has been extended to a spin-rotation invariant description [18,19], including Gaussian fluctuations [20–22], and refer to it shortly as slave bosons from here on.

In the slave-boson treatment, one replaces the fermionic creation and annihilation operators by a new set of fermionic ones combined with an auxiliary bosonic field. The bosonic fields are chosen such that the fermionic interaction terms are replaced by quadratic bosonic terms in the action, while the resulting pseudofermionic fields also only enter quadratically. When *local* constraints are imposed through Lagrange multiplier fields to constrain the values of bosonic fields to physical ones, one obtains an exact representation of the original problem. We employ a mean-field approximation for the bosonic fields, which imposes the constraints on average and allows for magnetic and nonmagnetic solutions. Following Ref. [22], one can acquire the expressions with the physical information of the original system, e.g., effective mass, spin, and charge susceptibility. Together with the periodic Anderson model, Kondo systems have been considered as a particularly suitable target to prove the accuracy of slave bosons for their physics including interacting electrons as well as hybridized orbitals.

In this work, we numerically implement the analytical representations from the slave-boson formalism and present the phase diagram for a model that resembles the low-energy physics in SmB_6 , but can be seen as paradigmatic for generic three-dimensional Kondo models with cubic and time-reversal symmetry. We find a total of seven phases, which are magnetically or topologically distinct, by tuning the strength of the electron-electron interactions as well as the on-site energy of the f electrons. Besides various PM insulating topological

*rthomale@physik.uni-wuerzburg.de

†titus.neupert@uzh.ch

phases, we find two topologically distinct insulating phases with (π, π, π) (Neel-)AFM order.

Model and method. We start with a short exposition of our model and the main ingredients of the spin-rotation invariant slave-boson formalism. The Hamiltonian introduced in Ref. [23] as a minimal model for SmB₆ reads

$$H = H_0 + H_{\text{hyb}} + H_{\text{int}}, \quad (1)$$

$$\begin{aligned} H_0 &= \sum_i \tilde{f}_i^\dagger \epsilon_f \tilde{f}_i - \sum_{\langle(i,j)\rangle} (\tilde{f}_i^\dagger t^f \tilde{f}_j + \mathbf{c}_i^\dagger t^d \mathbf{c}_j + \text{H.c.}) \\ &\quad - \sum_{\langle\langle(i,j)\rangle\rangle} (\tilde{f}_i^\dagger t^{f'} \tilde{f}_j + \mathbf{c}_i^\dagger t^{d'} \mathbf{c}_j + \text{H.c.}) - \sum_i \mu_0 \tilde{n}_i, \\ H_{\text{hyb}} &= \sum_\alpha \sum_{\langle(i,j)\rangle_\alpha} iV (\tilde{f}_i^\dagger \tau^\alpha \mathbf{c}_j + \mathbf{c}_i^\dagger \tau^\alpha \tilde{f}_j + \text{H.c.}), \\ H_{\text{int}} &= U \sum_i \tilde{f}_{i,\uparrow}^\dagger \tilde{f}_{i,\uparrow} \tilde{f}_{i,\downarrow}^\dagger \tilde{f}_{i,\downarrow} \end{aligned}$$

representing f - and d -electron hopping on a simple cubic lattice, their hybridization, and the local repulsive Hubbard interaction, respectively. The spinors $\tilde{f}_i^\dagger := (\tilde{f}_{i,\uparrow}^\dagger, \tilde{f}_{i,\downarrow}^\dagger)$ and $\mathbf{c}_i^\dagger = (c_{i,\uparrow}^\dagger, c_{i,\downarrow}^\dagger)$ are formed by the creation operators of d - (f -) electrons $c_{i,\sigma}^\dagger$ ($\tilde{f}_{i,\sigma}^\dagger$) with spin $\sigma \in \{\uparrow, \downarrow\}$, and $\tilde{n}_i = \tilde{f}_{i,\uparrow}^\dagger \tilde{f}_{i,\uparrow} + c_{i,\uparrow}^\dagger c_{i,\uparrow}$ represents the local density of all electrons at site i . We denote by $\langle(i,j)\rangle_\alpha$ a nearest-neighbor bond in the α direction and τ^α as the α th component of the vector of Pauli matrices $\boldsymbol{\tau} := (\tau^1, \tau^2, \tau^3)$ acting in spin space. The notations for nearest-neighbor ($\langle\cdot\rangle$) and next-to-nearest-neighbor ($\langle\langle\cdot\rangle\rangle$) pairs of sites are adopted in conventional form.

Following Ref. [23], we consider a half-filled band structure throughout and choose $t^d = 1$, $t^f = -0.1$, $t^{d'} = -0.4$, $t^{f'} = 0.04$, and $V = 0.5$; all energy scales will be given in units of t^d . The form of Eq. (1) and the chosen parameters account for negligible interactions as well as bigger hopping amplitudes among the d electrons as compared to the f electrons. We chose the relative energy shift between f - and d -orbitals ϵ_f and the interaction strength U as free parameters as a function of which we will map out the phase diagram. We complement simplified slave-boson studies, which did not consider the possibility of magnetic order [23] or were performed at infinite interaction U [24].

Slave-boson representation. To account for interactions, we apply the slave-boson representation of the operators $\tilde{f}_i^{(\dagger)}$, originally introduced by Kotliar and Ruckenstein [17], which has been generalized to be spin-rotation invariant (SRI) [18,19] and to consider fluctuations around the PM saddle point [20,21]. We introduce the bosonic fields $e_i, d_i, p_{i,0}$ and $\mathbf{p}_i := (p_{i,1}, p_{i,2}, p_{i,3})$, labeling empty, doubly, and singly occupied states, respectively, i.e.,

$$\begin{aligned} e_i^\dagger |\text{vac}\rangle &:= |\widetilde{\text{vac}}\rangle, \quad d_i^\dagger \tilde{f}_{i,\uparrow}^\dagger \tilde{f}_{i,\downarrow}^\dagger |\text{vac}\rangle := \tilde{f}_{i,\uparrow}^\dagger \tilde{f}_{i,\downarrow}^\dagger |\widetilde{\text{vac}}\rangle, \\ \frac{1}{2} \sum_{\tilde{\alpha}=0}^3 \sum_{\sigma'} (p_{i,\tilde{\alpha}}^\dagger \tau^{\tilde{\alpha}})_{\sigma\sigma'} \tilde{f}_{i,\sigma'}^\dagger |\text{vac}\rangle &:= \tilde{f}_{i,\sigma}^\dagger |\widetilde{\text{vac}}\rangle, \end{aligned} \quad (2)$$

with $|\text{vac}\rangle$ being the vacuum of the slave-boson representation containing a new set of auxiliary fermionic operators

$\tilde{f}_i^\dagger := (f_{i,\uparrow}^\dagger, f_{i,\downarrow}^\dagger)$. The unity matrix is denoted by τ^0 . The Hilbert space defined by the slave particle operators has to be projected onto the physical Hilbert space by the application of constraints (see Supplemental Material [25]), which are inserted via Lagrange multiplier terms in the Lagrangian by introducing five new fields $i\alpha_i, i\beta_{i,0}$, and $i\beta_{i,\alpha}$ per site i .

Mean-field approximation. We apply a mean-field ansatz, incorporating a static spin spiral with ordering vector \mathbf{Q} of a possible magnetic ground state. Following Ref. [26], we replace the bosonic fields at the lattice site labeled by i with lattice vector \mathbf{r}_i by $b_i \rightarrow b$, where b_i represents any of the fields $e_i, d_i, p_{0,i}, \alpha_i, \beta_{0,i}$, and define

$$\mathbf{p}_i \rightarrow \begin{pmatrix} \cos(\phi_i) \\ \sin(\phi_i) \\ 0 \end{pmatrix} p, \quad \text{and} \quad i\beta_i \rightarrow \begin{pmatrix} \cos(\phi_i) \\ \sin(\phi_i) \\ 0 \end{pmatrix} \beta. \quad (3)$$

Here, we have $\phi_i = \mathbf{Q} \cdot \mathbf{r}_i$, $\beta \in \mathbb{R}$ and $b, p \in \mathbb{R}_0^+$. Within this mean-field ansatz, the free energy per site is given by [25]

$$\begin{aligned} \frac{F}{N} &= -\frac{T}{N} \sum_{\nu=1}^8 \sum_k \ln [1 + e^{-\epsilon_{k,\nu}^\nu/T}] + U d^2 \\ &\quad + n\mu_0 - \beta_0(2d^2 + p^2 + p_0^2) - 2\beta p_0 p, \end{aligned} \quad (4)$$

where $\epsilon_{k,\nu}^\nu$ are the renormalized eigenvalues of the effective mean-field Hamiltonian, which implicitly depend on the slave-boson fields, and T is the temperature. The index ν is a combined label for the spin, orbital, and sublattice degrees of freedom. The filling is fixed at $n = 2$. As shown in Ref. [25], the free energy F is invariant under global SO(3) rotations of \mathbf{p}_i .

We distinguish mean-field solutions with $p = 0$, describing a PM state, and $p \neq 0$, signaling magnetic order. They are obtained by minimizing the free energy with respect to d, p_0 , and p , while maximizing with respect to β, β_0 , and μ_0 . Since there is a plethora of possible ordering vectors \mathbf{Q} to consider, we first calculate the PM mean field by explicitly setting $p = \beta = 0$ and then perform a stability analysis of the saddle point by expanding the action S up to second order in fluctuations of the bosonic fields.

Fluctuations around the paramagnetic saddle point. Within this expansion, the charge and spin susceptibility in momentum space are obtained as

$$\begin{aligned} \chi_c(q) &:= \langle \delta n_f(-q) \delta n_f(q) \rangle, \\ \chi_s^{\alpha\beta}(q) &:= \langle \delta S^\alpha(-q) \delta S^\beta(q) \rangle, \end{aligned} \quad (5)$$

where $S^\alpha = p_0 p_\alpha$ represents the spin density operator projected to direction α and $n_f = 2d^2 + p_0^2 + \mathbf{p}^2$ is the charge density operator expressed in bosonic fields. We find $\chi_s^{\alpha\beta}(q)$ to be proportional to the unit matrix and will hence refer to it as a scalar function $\chi_s(q)$ [22]. Here, $q := (\mathbf{q}, \omega)$ is the four-vector of the wave vector \mathbf{q} and frequency ω , and $\langle\cdot\rangle$ is the thermal expectation value of Gaussian fluctuations around the saddle point. We adopt the expressions for the susceptibilities from Refs. [22,27]. A sign change in the real part in the zero-frequency limit signals the onset of spontaneous charge or magnetic order. In the explored parameter domain, we do not find any charge instabilities. However, the real part of χ_s exhibits a sign change in the two-dimensional parameter space

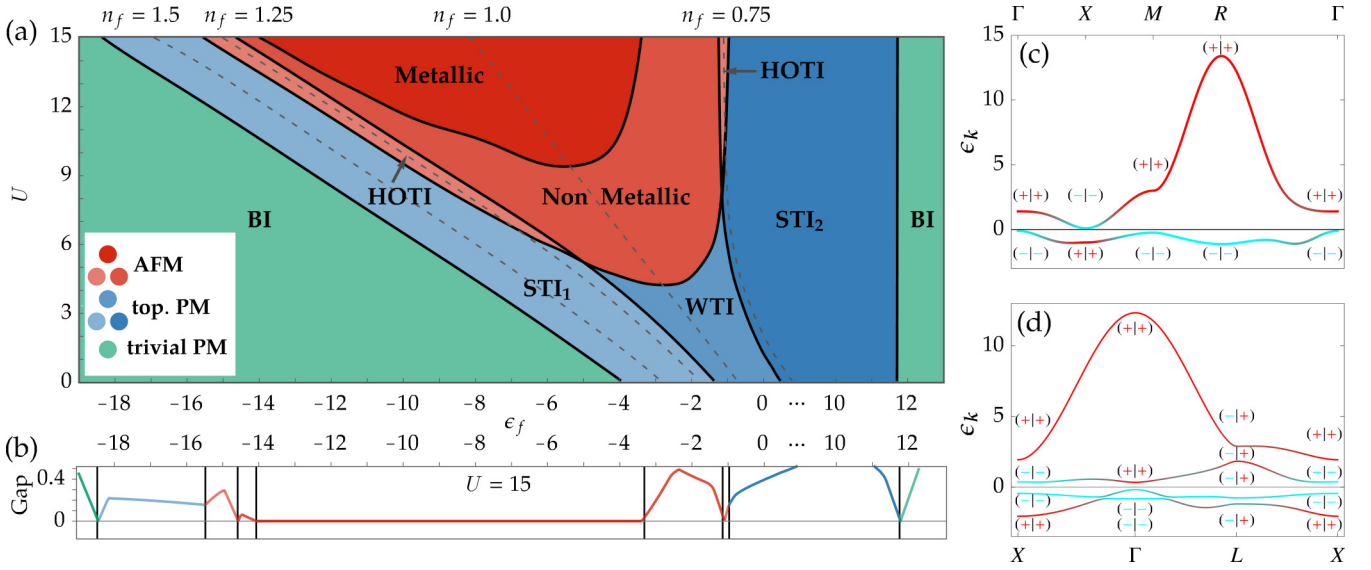


FIG. 1. (a) Topological phase diagram in the parameter space of (ϵ_f, U) . BI, WTI, STI_1 , and STI_2 phases are found in the PM region, whereas Non Metallic, Metallic, and HOTI phases appear in the AFM region. The phase boundaries are indicated by solid black lines. We further show trajectories of equal f -electron filling $n_f = 1.5, 1.25, 1.0, 0.75$ as dashed gray lines. (b) Gap plot as a function of ϵ_f for $U = 15$ featuring topological gap closings as well as the metallic AFM region. (c) Bulk band structure for $\epsilon_f = -12$ and $U = 10$ (STI_1) on the high-symmetry path Γ - X - M - R - Γ in the first BZ of the simple cubic lattice. (d) Bulk band structure for $\epsilon_f = -12$ and $U = 12$ (HOTI, AFM) on the high-symmetry path X - Γ - L - X in the first BZ of the face-centered-cubic lattice. Cyan (red) colored lines represent strong f (c) occupation and $(+|-)$ the inversion eigenvalues of each Kramer's pair. Red band weights in the occupied spectrum of (c) and (d) indicate band inversion.

(ϵ_f, U) , implying magnetic order. We compare the critical U at vanishing ω for the instability with $\mathbf{q} = (\pi, \pi, \pi)$ to that of other ordering vectors. None of the latter led to an instability at smaller U , and thus we conclude that the magnetic ordering vector is $\mathbf{Q} = (\pi, \pi, \pi)$ (see Ref. [25]). The magnetic phase boundary can be seen in Fig. 1, containing a magnetic region approximately bound by the f -electron fillings $n_f = 0.75$ and $n_f = 1.25$ for interactions larger than $U = 5$. The AFM mean-field spectrum allows for an insulator-to-metal transition by pushing noninteracting d electrons to the Fermi level, which emerges at large U around $n_f = 1$. Investigating possible (incommensurate) magnetic or charge instabilities which could emerge on the AFM band structure deeper in the phase would require a susceptibility analysis of the magnetic band structure, which is beyond the scope of this Rapid Communication. A general form of the mean-field Hamiltonian for arbitrary ordering vector \mathbf{Q} is derived in Ref. [25].

Topology of PM and AFM band structures. The solutions of the mean-field equations for $\mathbf{Q} = (\pi, \pi, \pi)$ yield magnetic and nonmagnetic domains in the parameter space of (ϵ_f, U) . The resulting PM phase boundary coincides with the one obtained by analyzing the fluctuations around the paramagnetic saddle point, separating the phase diagram in a PM (green/blue) and AFM (red) domain in Fig. 1. The remaining phase boundaries indicate either a change of topology or a metal-to-insulator transition.

Using the renormalized band structure, we can study the band topology. In the PM case, the effective hopping Hamiltonian (see Ref. [25]) features antiunitary time reversal $\mathcal{T} : (\mathcal{T}c_{\sigma,k}^{(\dagger)}\mathcal{T}^{-1}, \mathcal{T}f_{\sigma,k}^{(\dagger)}\mathcal{T}^{-1}) \mapsto (\sigma c_{-\sigma,-k}^{(\dagger)}, \sigma f_{-\sigma,-k}^{(\dagger)})$ and unitary inversion $\mathcal{I} : (\mathcal{I}c_{\sigma,k}^{(\dagger)}\mathcal{I}^{-1}, \mathcal{I}f_{\sigma,k}^{(\dagger)}\mathcal{I}^{-1}) \mapsto (c_{\sigma,-k}^{(\dagger)}, -f_{\sigma,-k}^{(\dagger)})$

symmetry, where $c_{\sigma,-k}^{(\dagger)}$ represents any fermionic operator with quantum numbers $(\sigma, -\mathbf{k})$. Because $(\mathcal{I}\mathcal{T})^2 = -1$, bands are doubly degenerate at every \mathbf{k} . We can define the \mathbb{Z}_2 -valued strong (ν_0^{PM}) and weak (ν_α^{PM}) topological indices [23,28–30]:

$$\text{strong: } \prod_{j=1}^8 \prod_{n \in \text{occupied}} \xi[n, \Gamma_j] = (-1)^{\nu_0^{\text{PM}}}, \quad (6)$$

$$\text{weak: } \prod_{j:k_\alpha=\pi} \prod_{n \in \text{occupied}} \xi[n, \Gamma_j] = (-1)^{\nu_\alpha^{\text{PM}}}. \quad (7)$$

Here, Γ_j represents the time-reversal-invariant momenta (TRIM), which are $\Gamma^{\text{PM}} = (0, 0, 0)$, $X^{\text{PM}} \in \{(\pi, 0, 0), (0, \pi, 0), (0, 0, \pi)\}$, $M^{\text{PM}} \in \{(\pi, \pi, 0), (0, \pi, \pi), (\pi, 0, \pi)\}$, and $R^{\text{PM}} = (\pi, \pi, \pi)$ in the first Brillouin zone (BZ) of the simple cubic lattice. $\xi[n, \Gamma_j]$ is the inversion eigenvalue of the n th Kramer's pair at the Γ_j point. Due to the cubic symmetry in the PM phase, all the weak indices are equivalent, i.e., $\nu_x^{\text{PM}} = \nu_y^{\text{PM}} = \nu_z^{\text{PM}}$. Therefore, we can maximally have four topologically distinct phases given by $(\nu_0^{\text{PM}}, \nu_\alpha^{\text{PM}}) \in \{(0, 0), (0, 1), (1, 0), (1, 1)\}$. We denote these phases by band insulator (BI), weak topological insulator (WTI) and strong topological insulator of type one and two (STI_1, STI_2), respectively. We illustrate the factors of the strong index ν_0^{PM} for the STI_1 phase at $(\epsilon_f, U) = (-12, 10)$ in Fig. 1(c): the eigenvalues $\xi[1, \Gamma_j]$ are -1 ($+1$) for the blue- (red)-colored portions of the energy bands, such that $\xi[1, \Gamma^{\text{PM}}] = \xi[1, M^{\text{PM}}] = \xi[1, R^{\text{PM}}] = -1$, but $\xi[1, X^{\text{PM}}] = 1$ and, consequently, $\nu_0^{\text{PM}} = 1$.

In the magnetically ordered phases with ordering vector $\mathbf{Q} = (\pi, \pi, \pi)$, the real-space primitive unit cell is doubled in size since each site i is surrounded by six neighboring

sites with opposite spin expectation value. In this AFM phase, the system has a pseudo-time-reversal symmetry \mathcal{T}' as the combination of \mathcal{T} and the translation by \hat{r}_α to a nearest neighbor in the α direction. Moreover, inversion symmetry \mathcal{I} is retained. We find four doubly degenerate bands. The change in the unit cell from simple cubic to face-centered cubic results in eight new TRIMs, which are $\Gamma := 0$, $L := \mathbf{b}_1/2$, $X := (\mathbf{b}_1 + \mathbf{b}_2)/2$. Of these, L and X have, respectively, four and three partners obtained by C_4 rotations. Here, $\mathbf{b}_1 := (-\pi, \pi, \pi)$, $\mathbf{b}_2 := (\pi, -\pi, \pi)$, and $\mathbf{b}_3 := (\pi, \pi, -\pi)$ in units of $|\hat{r}_\alpha|^{-1}$ are the three primitive reciprocal lattice vectors of the fcc structure. Hence, the strong index,

$$\nu^{\text{AFM}} : \prod_{n \in \text{occupied}} \xi[n, \Gamma] \xi[n, X] = (-1)^{\nu^{\text{AFM}}}, \quad (8)$$

corresponding to Eq. (7) remains \mathbb{Z}_2 valued, with the four L points always yielding a trivial contribution. As shown in Fig. 1, each Kramer's pair at the L point has two different inversion eigenvalues. Due to the translation operator in \mathcal{T}' , which does not commute with the inversion operator at L , we find the relative phase between the eigenvalues of the two pairs to be $\exp(2i\hat{r}_\alpha L) = -1$. Thus, the weak index

$$\nu_{\text{weak}}^{\text{AFM}} : \prod_{n \in \text{occupied}} (\xi[n, X])^2 = 1 = (-1)^{\nu_{\text{weak}}^{\text{AFM}}} \quad (9)$$

is always trivial. Therefore, apart from the metallic regime, we find a region with the trivial topological index $\nu^{\text{AFM}} = 0$, which is labeled Non Metallic, and a higher-order topological insulator (HOTI) $\nu^{\text{AFM}} = 1$, exhibiting topological states in two dimensions lower than the bulk [31–37]. We illustrate the factors of the index ν^{AFM} for the HOTI phase at $(\epsilon_f, U) = (-12, 12)$ in Fig. 1(d).

The phase with nontrivial topology can further be classified as an axion insulator (AXI), which, depending on the orientation of the surfaces, can show gapless chiral hinge modes while the surface and bulk remain gapped. These modes are realized in a geometry that preserves \mathcal{I} and breaks \mathcal{T}' . Experimental evidence for such magnetically ordered topological materials was recently observed in MnBi_2Te_4 and Bi_2Se_3 thin films [38–40]. The hinge modes in a nanowire geometry are shown in Fig. 2. Surfaces that preserve \mathcal{T}' would feature a gapless Dirac cone.

Phase diagram. To sum up, depending on the parameter set (ϵ_f, U) that we probe, the effective fermionic part of Eq. (1) can realize a PM or an AFM phase with ordering vector $\mathbf{Q} = (\pi, \pi, \pi)$. There are four topologically distinct subphases (BI, WTI, STI_1 , and STI_2) in the PM phase, which are determined by the two topological indices ν_0^{PM} and ν_α^{PM} . On the other hand, there are three subphases (metallic, nonmetallic, and HOTI) in the AFM region. We find that the nonmetallic AFM phase features surface states, which are not topologically protected.

We further investigate the possibility of obtaining excitonic states with our formalism [25]. These charge-neutral collective modes have been suggested to account for the longstanding anomalies in SmB_6 in several experimental observations and point to the relevance of excitons for the electronic structure of SmB_6 [41,42]. However, we do not find any

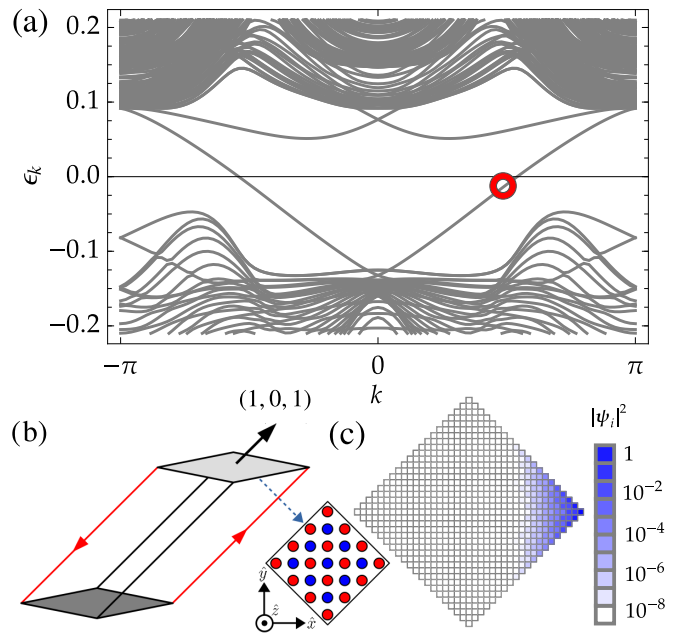


FIG. 2. (a) Band structure in the inclined column geometry depicted in (b) at $(\epsilon_f, U) = (-12, 12)$ featuring chiral hinge modes. (b) An example of column geometry where the hinge mode appears. The AFM spin texture in each plane is shown in the diamond-shaped inset. Red (blue) circles indicate spin \downarrow (\uparrow) in the fermionic part of the renormalized Hamiltonian. (c) Probability distribution in real space of the hinge state indicated in (a) by the red circle. $20 \times 20 + 19 \times 19 = 761$ sites are used for the plot.

evidence for excitonic states or bands separated from the band continuum within the dynamical spin susceptibility within our slave-boson treatment.

Conclusion. We studied the phase diagram of a paradigmatic model for three-dimensional TKIs using the scheme of Kotliar-Ruckenstein's slave-boson representation. To that end, we numerically implemented the analytical expressions of charge and spin susceptibility of a cubic and time-reversal symmetric system. We obtained a collection of phases in which topological properties and magnetic symmetry breaking are intertwined, yielding, among others, an axion insulator with chiral hinge modes.

Previous studies have theoretically predicted a bulk band inversion of SmB_6 at the X point and surface Dirac cones at the \bar{X} and $\bar{\Gamma}$ points of the surface BZ [23,43,44], which have been observed experimentally [45]. These characteristics coincide with the STI_1 phase in our phase diagram. Further SmB_6 shows strong indications of AFM ordering under pressure [9,15], which is all captured in our minimal model within a small parameter range of (ϵ_f, U) , corresponding to f -electron fillings n_f between 1.5 and 1.25. Judging from our results, we expect an indication of the sequence of phase transitions STI_1 to HOTI to nonmetallic AFM in the specific heat as a function of pressure, which could be of interest to future experimental investigations.

Acknowledgments. The authors at the University of Zurich acknowledge support from the Swiss National Science Foundation (Grant No. 200021_169061) and from the European Unions Horizon 2020 research and innovation program

(Grant No. ERC-StG-Neupert-757867-PARATOP). The work in Würzburg is funded by the Deutsche Forschungsgemeinschaft (DFG, German Research Foundation) through Project-ID No. 258499086-SFB 1170 and through the Würzburg-Dresden Cluster of Excellence on Complexity and Topology

in Quantum Matter – *ct.qmat* Project-ID No. 39085490-EXC 2147. The authors also gratefully acknowledge the support of Markus Legner and Jannis Seufert.

The authors M.K., S.O., and D.R. contributed equally to this work.

- [1] M. Dzero, K. Sun, V. Galitski, and P. Coleman, *Phys. Rev. Lett.* **104**, 106408 (2010).
- [2] M. Dzero, J. Xia, V. Galitski, and P. Coleman, *Annu. Rev. Condens. Matter Phys.* **7**, 249 (2016).
- [3] P. Nikolić, *Phys. Rev. B* **90**, 235107 (2014).
- [4] V. Alexandrov, P. Coleman, and O. Erten, *Phys. Rev. Lett.* **114**, 177202 (2015).
- [5] B. Roy, J. Hofmann, V. Stanev, J. D. Sau, and V. Galitski, *Phys. Rev. B* **92**, 245431 (2015).
- [6] Y. Nakajima, P. Syers, X. Wang, R. Wang, and J. Paglione, *Nat. Phys.* **12**, 213 (2016).
- [7] A. Thomson and S. Sachdev, *Phys. Rev. B* **93**, 125103 (2016).
- [8] K.-W. Chang and P.-J. Chen, *Phys. Rev. B* **97**, 195145 (2018).
- [9] Y. Zhou, Q. Wu, P. F. Rosa, R. Yu, J. Guo, W. Yi, S. Zhang, Z. Wang, H. Wang, S. Cai, K. Yang, A. Li, Z. Jiang, S. Zhang, X. Wei, Y. Huang, P. Sun, Y. feng Yang, Z. Fisk, Q. Si, Z. Zhao, and L. Sun, *Sci. Bull.* **62**, 1439 (2017).
- [10] I. Berman, N. Brandt, V. Moshchalkov, S. Pashkevich, V. Sidorov, E. Konovalova, and Y. Paderno, *JETP Lett.* **38**, 477 (1983).
- [11] J. Beille, M. B. Maple, J. Wittig, Z. Fisk, and L. E. DeLong, *Phys. Rev. B* **28**, 7397(R) (1983).
- [12] S. Gabáni, E. Bauer, M. Della Mea, K. Flachbart, Y. Paderno, V. Pavlík, and N. Shitsevalova, *J. Magn. Magn. Mater.* **272**, 397 (2004).
- [13] P. K. Biswas, Z. Salman, T. Neupert, E. Morenzeni, E. Pomjakushina, F. von Rohr, K. Conder, G. Balakrishnan, M. C. Hatnean, M. R. Lees, D. M. Paul, A. Schilling, C. Baines, H. Luetkens, R. Khasanov, and A. Amato, *Phys. Rev. B* **89**, 161107(R) (2014).
- [14] W. T. Fuhrman, J. Leiner, P. Nikolić, G. E. Granroth, M. B. Stone, M. D. Lumsden, L. DeBeer-Schmitt, P. A. Alekseev, J.-M. Mignot, S. M. Koohpayeh, P. Cottingham, W. A. Phelan, L. Schoop, T. M. McQueen, and C. Broholm, *Phys. Rev. Lett.* **114**, 036401 (2015).
- [15] A. Barla, J. Derr, J. P. Sanchez, B. Salce, G. Lapertot, B. P. Doyle, R. Rüffer, R. Lengsdorf, M. M. Abd-Elmeguid, and J. Flouquet, *Phys. Rev. Lett.* **94**, 166401 (2005).
- [16] P. Alekseev, V. Lazukov, K. Nemkovski, and I. Sadikov, *J. Expt. Theor. Phys.* **111**, 285 (2010).
- [17] G. Kotliar and A. E. Ruckenstein, *Phys. Rev. Lett.* **57**, 1362 (1986).
- [18] T. Li, P. Wölfle, and P. J. Hirschfeld, *Phys. Rev. B* **40**, 6817 (1989).
- [19] R. Frésard and P. Wölfle, *Int. J. Mod. Phys. B* **06**, 685 (1992).
- [20] T. Li, Y. S. Sun, and P. Wölfle, *Z. Phys. B Condens. Matter* **82**, 369 (1991).
- [21] W. Zimmermann, R. Frésard, and P. Wölfle, *Phys. Rev. B* **56**, 10097 (1997).
- [22] M. Klett, D. Riegler, T. Neupert, R. Thomale, and P. Wölfle (unpublished).
- [23] M. Legner, A. Rüegg, and M. Sigrist, *Phys. Rev. B* **89**, 085110 (2014).
- [24] H. Li, Y. Zhong, Y. Liu, H.-G. Luo, and H.-F. Song, *J. Phys.: Condens. Matter* **30**, 435601 (2018).
- [25] See Supplemental Material at <http://link.aps.org/supplemental/10.1103/PhysRevB.101.161112> for more details.
- [26] B. Möller and P. Wölfle, *Phys. Rev. B* **48**, 10320 (1993).
- [27] D. Riegler, M. Klett, T. Neupert, R. Thomale, and P. Wölfle, [arXiv:1912.07631](https://arxiv.org/abs/1912.07631).
- [28] L. Fu and C. L. Kane, *Phys. Rev. B* **76**, 045302 (2007).
- [29] L. Fu, C. L. Kane, and E. J. Mele, *Phys. Rev. Lett.* **98**, 106803 (2007).
- [30] X.-L. Qi, T. L. Hughes, and S.-C. Zhang, *Phys. Rev. B* **78**, 195424 (2008).
- [31] A. M. Essin, J. E. Moore, and D. Vanderbilt, *Phys. Rev. Lett.* **102**, 146805 (2009).
- [32] R. S. K. Mong, A. M. Essin, and J. E. Moore, *Phys. Rev. B* **81**, 245209 (2010).
- [33] F. Schindler, A. M. Cook, M. G. Vergniory, Z. Wang, S. S. P. Parkin, B. A. Bernevig, and T. Neupert, *Sci. Adv.* **4**, eaat0346 (2018).
- [34] J. Ahn and B.-J. Yang, *Phys. Rev. B* **99**, 235125 (2019).
- [35] J. Langbehn, Y. Peng, L. Trifunovic, F. von Oppen, and P. W. Brouwer, *Phys. Rev. Lett.* **119**, 246401 (2017).
- [36] C. Yue, Y. Xu, Z. Song, H. Weng, Y.-M. Lu, C. Fang, and X. Dai, *Nat. Phys.* **15**, 577 (2019).
- [37] R.-X. Zhang, F. Wu, and S. D. Sarma, *Phys. Rev. Lett.* **124**, 136407 (2020).
- [38] M. M. Otrokov, I. I. Klimovskikh, H. Bentmann, D. Estyunin, A. Zeugner, Z. S. Aliev, S. Gaß, A. U. B. Wolter, A. V. Koroleva, A. M. Shikin *et al.*, *Nature (London)* **576**, 416 (2019).
- [39] Y. Gong, J. Guo, J. Li, K. Zhu, M. Liao, X. Liu, Q. Zhang, L. Gu, L. Tang, X. Feng *et al.*, *Chin. Phys. Lett.* **36**, 076801 (2019).
- [40] S.-Y. Xu, M. Neupane, C. Liu, D. Zhang, A. Richardella, L. A. Wray, N. Alidoust, M. Leandersson, T. Balasubramanian, J. Sánchez-Barriga *et al.*, *Nat. Phys.* **8**, 616 (2012).
- [41] H. Ohta, R. Tanaka, M. Motokawa, S. Kunii, and T. Kasuya, *J. Phys. Soc. Jpn.* **60**, 1361 (1991).
- [42] J. Knolle and N. R. Cooper, *Phys. Rev. Lett.* **118**, 096604 (2017).
- [43] T. Takimoto, *J. Phys. Soc. Jpn.* **80**, 123710 (2011).
- [44] F. Lu, J. Z. Zhao, H. Weng, Z. Fang, and X. Dai, *Phys. Rev. Lett.* **110**, 096401 (2013).
- [45] N. Xu, P. Biswas, H. Dil, R. Dhaka, G. Landolt, S. Muff, C. Matt, Y. Wang, N. Plumb, M. Radovic, E. Pomjakushina, K. Conder, A. Amato, S. Borisenko, R. Yu, H. Weng, Z. Fang, X. Dai, J. Mesot, and M. Shi, *Nat. Commun.* **5**, 4566 (2014).